---

*Archives of Razi Institute Journal*

*Volume 80, NO. 4, 2025*

**Journal homepage:** https://archrazi.areeo.ac.ir

**Original Article**

# The Antimicrobial and Antibiofilm Potential of *Citrus Aurantium* and *Artemisia Annua* Essential Oils Nanoemulsions

**Mahmoud Osanloo[1], Hiva Alipanah[2], Mohammad Arman Hashempour[3], Benyamin Motazedian[3], Elham Zarenezhad[4], Zahra Zahedifard[5], Abdolmajid Ghasemian[4*]**

*1.Department of Medical Nanotechnology, School of Advanced Technologies in Medicine, Fasa University of Medical Sciences, Fasa, Iran*
*2.Department of Physiology, School of Medicine, Fasa University of Medical Sciences, Fasa, Iran*
*3.Department of Medicine, School of Medicine, Fasa University of Medical Sciences, Fasa, Iran*
*4.Noncommunicable Diseases Research Center, Fasa University of Medical Sciences, Fasa, Iran*
*5.Department of Medical Biotechnology, School of Advanced Technologies in Medicine, Fasa University of Medical Sciences, Fasa, Iran.*

**Article Info:**

**Received:** 8 May 2024
**Revised:** 20 August 2024
**Accepted:** 22 September 2024

**Keywords:**

Antibacterial Agents,
Essential Oil,
Reactive Oxygen Species,
Phytochemicals.

## ABSTRACT

Antimicrobial resistance has posed considerable health and economic burdens globally (approximately five million deaths annually), particularly in developing countries. The estimated annual treatment costs in the United States include US$4.6 billion. Vast antibiotic resistance among Gram-negative and Gram-positive bacterial species has spread from healthcare to the environment, community, and animals. These conditions have limited and in some cases, failed infection eradication options and facilitated the distribution of drug-resistant organisms. The spread of drug-resistant bacterial infections is a major human health concern, hence, seeking novel antibacterial agents is crucial. This study used nanoemulsions of *Citrus aurantium* and *Artemisia annua* essential oils (EOs) as natural antibacterial agents. Gas chromatography mass spectrometry (GC–MS) analysis showed that limonene (31.4%) and artemisia ketone (26.2%) were major components, respectively. After that, their nanoemulsion dosage forms with mean droplet sizes of 181 ± 7 and 160 ± 5 and zeta potential values 3.1 ± 0.8 and -4.9 ± 0.5 mV were prepared. Meanwhile, successful loading of the EOs in nanoemulsion was confirmed by Attenuated Total Reflection-Fourier Transform Infrared (ATR-FTIR) analysis. *A. annua* nanoemulsion with 40% antioxidant effect was significantly more potent than *C. aurantium* nanoemulsion. Meanwhile, nanoemulsions' antibacterial and antibiofilm activity against clinical and standard strains, *Escherichia coli*, *Staphylococcus aureus*, *Pseudomonas aeruginosa*, and *Klebsiella pneumonia*, were investigated. The best efficiency was related to the effect of *C. aurantium* nanoemulsion against *S. aureus*; minimum inhibitory (MIC) and minimum bactericidal concentrations (MBC) were 500 and > 2000 µg/mL. In addition, no biofilm was formed after treatment with both nanoemulsions. Therefore, *C. aurantium* and *A. annua* EO nanoemulsions may act as natural antioxidant and antibacterial agents in complementary medicine.

**Corresponding Author:**
**majidghasemian86@gmail.com**

https://orcid.org/0000-0002-1243-6341
https://orcid.org/0000-0003-2805-1910

**How to cite this article:** **Osanloo M, Alipanah H, Hashempour MA, Motazedian B, Zarenezhad E, Zahedifard Z, Ghasemian A. The Antimicrobial and Antibiofilm Potential of Citrus Aurantium and Artemisia Annua Essential Oils Nanoemulsions. *Archives of Razi Institute*. 2025;80(4):927-936.** DOI: 10.32592/ARI.2025.80.4.927

## 1. Introduction

Vast antibiotic resistance among Gram-negative and Gram-positive bacteria has spread from healthcare to the environment, community, and animals. These conditions have limited ,and in some cases, failed the infection eradication options, facilitating the distribution of drug-resistant organisms (1, 2) such as those non-susceptible to last-resort antibiotics of carbapenems and glycopeptides. As alternatives to chemotherapies, natural resources such as essential oils (EOs) have been suitable alternatives (3-5). In addition, nanoformulation of EOs by optimization in particle size, increasing solubility, and improving bioavailability and stability causes medicines to be more permeable into cells, such as bacteria or cancer cells (6-10).

The *citrus* genus includes several species of citrons within the family *Rutaceae*, used as herbal medicines, fruits, juice, and additives. *Citrus* fruits contain vitamins C and B, minerals, nutrients, and bioactive compounds such as phenolic compounds, volatile oils, and terpenoids. *Citrus aurantium* (*C. aurantium*) L. cultivar has exhibited anti-inflammatory, hypoglycemic, antimicrobial, anticancer, pain-relief, and organ- protective effects (11). Although the species has bioactive compounds and biological activities, its pharmacological effects, traditional usage, and exact bioactive compounds have not been uncovered (12). On the other hand, *C. aurantium* L. dietary supplementation has not exerted side effects (13). Various extracts of *C. aurantium* L. leaves, including aqueous, alcoholic, or chloroform portions, have demonstrated antibacterial effects against various agents (11, 13).

In addition, the antimicrobial effects of its EOs have unraveled potential activities against *Agrobacterium tumefaciens*, *Dickeya solani*, and *Erwinia amylovora* (14, 15). *Artemisia annua* grows globally in Europe, Asia and North America with preferred arid and semi-arid climates and provides considerable health benefits such as anticancer and antimicrobial properties. Major aioactive compounds include artemisia ketone, 1,8-cineole, germacrene D, and camphor (16). This study aimed to investigate the antibacterial and antibiofilm effects of nanoemulsions of *A. annua* L. and *C. aurantium*.

## 2. Materials and Methods

### 2.1. Materials

*C. aurantium* and *A. annua* EOs were supplied from Iranian companies, Tabib Daru Company and Pharmaceutical Company Essential Oil Dr. Soleimani. Bacterial standard strains included *Escherichia coli* ATCC25922, *Staphylococcus aureus* ATCC25923, *Pseudomonas aeruginosa* ATCC 27853, and *Klebsiella pneumonia* ATCC13883 were cultured from bacterial stock preserved at -20 °C in the microbiology laboratory of Fasa University of Medical Sciences, Iran. Moreover, clinical isolates were also obtained from patients. Mueller Hinton broth, trypticase soy broth, crystal violet, tween 20, and tween 80 were purchased from Merck Chemicals, Germany. The standard analytical solution of Alkanes (C9-C24) was supplied from Sigma-Aldrich (USA).

### 2.2. Chemical Composition of Eos

Gas chromatography mass spectrometry (GC–MS) analysis was used for the chemical compositions of the EOs. For this purpose, the gas chromatographic device (Agilent 6890, USA) with HP-5MS silica fused columns coupled to a network mass selective detector (Agilent 5973, USA) was used. Major constituents of EOs were identified by comparing their retention indices to homologous C9-C24 n-alkanes, as previously described (17, 18).

### 2.3. Preparation and Characterizations of Nanoemulsions

*A. annua* EO (0.4% v/v) was mixed with tween 80 (0.5% v/v), and *C. aurantium* (0.4% v/v) was mixed with tween 20 (0.5% v/v), separately, for 3 minutes at room temperature at 2000 rpm. Distilled water was then added dropwise to reach the final volume of 5 mL, and the mixture was stirred for 40 minutes at room temperature at 2000 rpm. Droplet size and droplet size distribution (SPAN) were measured using a DLS (Dynamic Light Scattering, DLS9900, K-ONE, Korea) device. SPAN was calculated using the relationship d90-d10/d50; in this equation, d is the diameter, 90, 10, and 50 percent of particles with a size smaller than the values mentioned.

The droplet size below 200 nm and SPAN below 1 nm were necessary conditions to confirm the appropriate size characteristics. TEM (Transitional Electron Microscopy, Philips, TEM, EM 208s, Netherland) was used to confirm the droplet size and determine their morphology. ATR-FTIR (Attenuated Total Reflection-Fourier Transform Infrared) analysis is used to evaluate the successful loading of the EOs in the nanoemulsion. Spectra of the EOs, nanoemulsion (-oil), and nanoemulsion were

recorded in 400 - 4000 $cm^{-1}$ using a spectrometer (Tensor II model, Bruker Co, Germany).

Furthermore, the stability of nanoemulsions was investigated. Nanoemulsions were centrifuged at −4, +4, and +25°C (14,000 g, 30 min) to investigate stability against precipitation. Additionally, nanoemulsions were stored at +45°C and room temperature for six consecutive intervals of 48 hours for thermal stability analysis. Moreover, nanoemulsions were placed at −20°C and room temperature for six consecutive 48-hour intervals for cryogenic stability. In addition, nanoemulsions were placed at $4^0$C and room temperature for six months for long-term stability analysis. After each test, the nanoemulsion was visually checked for sedimentation, creaming, or phase separation.

**2.4. Investigation of Antioxidant Properties of EOs and Nanoemulsions**

DPPH (2,2-diphenyl-1-picrylhydrazyl) assay was used to measure antioxidant properties. First, serial dilutions of the nanoemulsions (62.5-2000 µg/mL) were prepared in ethanol. Next, 50 µL/well of each prepared dilution and 0.2 mM DPPH solution was added to a 96-well plate, and was incubated for 30 minutes in the dark at room temperature. Finally, the wells' OD (optical density) was measured at 517 nm using a plate reader (Synergy HTX Multi-Model Reader, USA). Antioxidant activity was calculated using OD test/OD control×100.

**2.5. Minimum Inhibitory Concentration**

Micro-dilution test was implemented. The range of concentrations of nanoemulsions (250, 500, 1000, 1500 and 2000 µg/mL) was prepared by PBS containing 0.5% DMSO as solvent. Antibacterial effects of EOs and nanoemulsion were investigated using 96-well broth micro-dilution, as previously described(19). Briefly, 40 µL of each was inoculated into wells of 96 well plates containing 50 µL of Mueller Hinton broth. Afterward, 10 µL/well of each bacterial suspension (0.5 McFarland standard turbidity, $1.5\times10^8$ CFU/mL) was added to each well. The plates were incubated for 24 hours at 37 ºC, and then the OD of the wells was read at 630 nm. Bacterial growth was calculated using OD sample/OD control×100. The minimum inhibitory concentration (MIC) of *A. annua* and *C. aurantium* single and nanoemulsion forms against bacterial strains were determined using concentrations ranging from 250-2000 µg/mL. Moreover, the bacterial suspension equal to 0.5 McFarland standard was prepared. The test was performed the same as the broth micro-dilution method.

**2.6. Biofilm Formation**

Anti-biofilm effects of EOs and nanoemulsions were assessed against clinical isolates. The biofilm formation with and without exposure to the nanoemulsions was performed into 96-well plates using a microtitre tissue plate assay. Briefly, an overnight culture of bacterial strains was obtained into the trypticase soy broth (TSB) medium containing 1% glucose and diluted 1:100. For each bacterial suspension, 20 µL was taken and inoculated into wells containing 180 µL of the TSB medium in triplicate and incubated for 5 hours for exposed (2000 µg/mL of each nanoemulsion) group and 24h for the unexposed group.

The unexposed group medium was exchanged with each nanoemulsion and incubated for 24 hours. Next, the wells were washed using double distilled water and fixed using methanol. Then, 0.1% crystal violet or safranin was added for 15 min. After washing, the absolute ethanol (200 µL) was added to solubilize bacterial contents and read using the ELISA reader at 490 nm. The biofilm formation levels (strong, moderate, weak, or non-adherence) were calculated using Table 1. This study compared biofilm formation levels among groups, including the control (unexposed) and *A. annua* and *C. aurantium* EOs nanoemulsion-treated groups.

**2.7. Data analysis**

All experiments were done in triplicates. The data were analyzed using the SPSS software, from which Chi-Square and analysis of variance (ANOVA) tests were applied to determine differences at a *p*-value cut-off of 0.05.

## 3. Results

The main components of the *C. aurantium* were limonene (31.4%), sabinene (15.6%), ɣ-terpinene (6.0%), linalool (5.6%) and cis-nerolidol (5.1%) (Table 2). Similarly, the main components of the *A. annua* were artemisia ketone (26.2%), camphor (19.2%), 1,8-cineole (12.3%), *trans*-caryophyllene (4.5%), and camphene (4.4%) (Table 2).

**3.1. TEM analysis of *C. Aurantium* and *A. Annua* EO Nanoemulsions**

The mean droplet diameter and zeta potential of *C. aurantium* nanoemulsion were 181 ± 7 nm and 3.1 ± 0.8 mV, respectively (Figures 1 A & B). The *A. annua* nanoemulsions exhibited a droplet diameter of 160 ± 5 nm and zeta potential values of -4.9 ± 0.5 mV (Figures 2 A & B).

**Table1.** The calculation of biofilm formation levels

| Biofilm formation ability | Calculation of cut-off level | OD calculated results | Reference |
|---|---|---|---|
| **Strong** | OD>ODc×4 | 0.33296>OD | (20, 21) |
| **Moderate** | ODc×2≤OD<ODc×4 | 0.16648≤OD<0.33296 | |
| **Weak** | ODc≤OD<2×ODc | 0.083324≤OD<0.16648 | |
| **No binding** | OD≤ODc | 0.08324≤OD | |

OD: optical density, ODc: mean OD of control wells.

**Table 2.** Identified compounds in the EOs using GC-MS analysis.

| Retention Time (min) | Compound | *C. aurantium* | | *A. annua* | | Retention Index |
|---|---|---|---|---|---|---|
| | | **Area** | **%** | **Area** | **%** | |
| **9.46** | α-pinene | 58484827 | 1.7 | 122296938 | 4.1 | 932 |
| **10.06** | camphene | -- | -- | 132788539 | 4.4 | 954 |
| **11.14** | sabinene | 542668432 | 15.6 | 44039171 | 1.5 | 975 |
| **11.24** | β-pinene | 43301938 | 1.2 | 29556997 | 1.0 | 979 |
| **11.96** | β-myrcene | 108784770 | 3.1 | 29379228 | 1.0 | 988 |
| **12.50** | Yomogi alcohol | -- | -- | 41103264 | 1.4 | 999 |
| **13.08** | α-terpinene | 59177141 | 1.7 | -- | -- | 1014 |
| **13.81** | 1,8-cineole | -- | -- | 368453758 | 12.3 | 1026 |
| **13.89** | limonene | 1088445097 | 31.4 | -- | -- | 1029 |
| **14.67** | *cis*-ocimene | 162728160 | 4.7 | -- | -- | 1037 |
| **15.13** | ɣ-terpinene | 207125216 | 6.0 | -- | -- | 1054 |
| **15.48** | artemisia ketone | -- | -- | 784989266 | 26.2 | 1062 |
| **16.31** | artemisia alcohol | -- | -- | 33487881 | 1.1 | 1083 |
| **17.16** | linalool | 192637034 | 5.6 | -- | -- | 1095 |
| **19.22** | camphor | -- | -- | 576552736 | 19.2 | 1146 |
| **20.12** | borneol | -- | -- | 28483988 | 1.0 | 1169 |
| **20.63** | 4-terpineol | 66692764 | 1.9 | 33586786 | 1.1 | 1177 |
| **23.55** | cuminic aldehyde | 128003231 | 3.7 | -- | -- | 1239 |
| **29.38** | α-copaene | -- | -- | 47639328 | 1.6 | 1376 |
| **31.26** | *trans*-caryophyllene | -- | -- | 136219018 | 4.5 | 1419 |
| **33.78** | germacrene D | -- | -- | 84811438 | 2.8 | 1481 |
| **33.99** | β-selinene | -- | -- | 90133377 | 3.0 | 1490 |
| **37.11** | *cis*-nerolidol | 178234586 | 5.1 | -- | -- | 1532 |
| **37.76** | caryophyllene oxide | -- | -- | 35663606 | 1.2 | 1583 |
| **42.89** | *cis*-farnesol | 34776356 | 1.0 | -- | -- | 1698 |

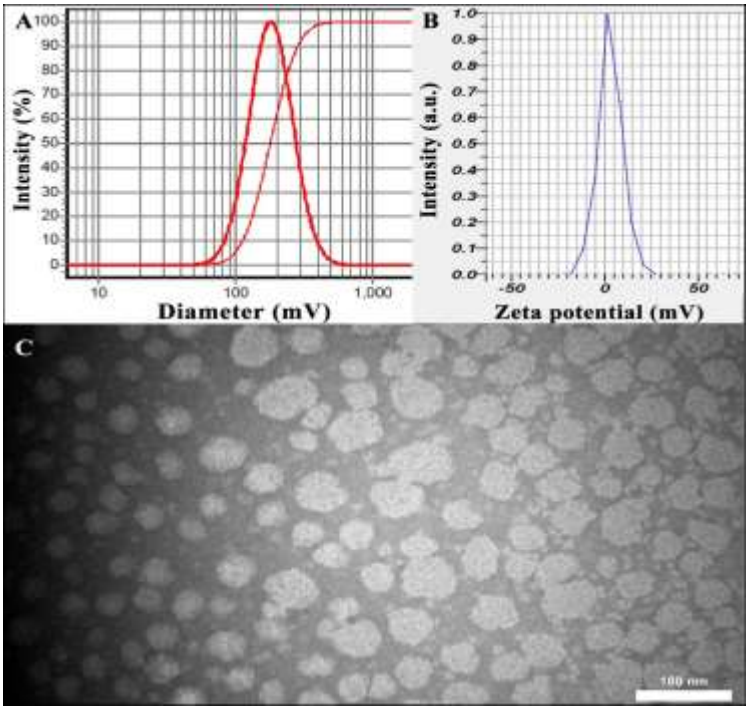


**Figure 1.** Characterization of *C. aurantium* EO nanoemulsion, A: DLS profile, B: zeta potential profile, and C: TEM image.

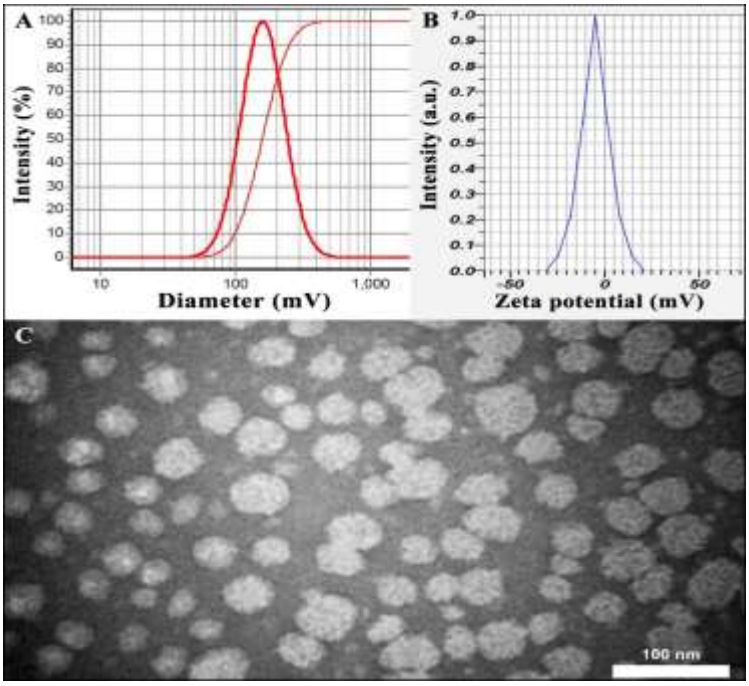


**Figure 2.** Characterization of *A. annua* EO nanoemulsion, A: DLS profile, B: zeta potential profile, and C: TEM image.

The TEM analysis (Figures 1C and 2C) revealed that both nanoemulsions were spherical in shape, with sizes < 100 nm. Furthermore, the stability of nanoemulsions was investigated.

They were centrifuged at −4, +4, and +25°C (14,000 g, 30 min); no sedimentation or phase separation was observed. Additionally, nanoemulsions were stored at +45°C and room temperature for six consecutive intervals of 48 hours for thermal stability analysis; no sedimentation or bi-phasic condition was observed.

Moreover, nanoemulsions were placed at −20°C and room temperature for six consecutive 48-hour intervals for cryogenic stability; no sedimentation or bi-phasic condition was observed. In addition, nanoemulsions were placed at 4 and room temperature for six months for long-term stability analysis; no sedimentation or phase separation was observed.

### 3.2. ATR-FTIR Analysis of *C. Aurantium* And *A. Annua* Nanoemulsions

ATR-FTIR analysis confirmed EO loading in nanoemulsion (Figure 3). The spectra of *C. aurantium*

EO ,displayed in Figure 3A, broadband at 3469 cm $^{-1}$ can be attributed to stretching vibration of the hydroxyl group due to hydrogen bonding in alcoholic and phenolic bioactive compounds in EO, spectra at 3076 cm$^{-1}$ can be corresponded to stretching vibration of CH in $sp^2$ groups and the bands at 2961, 2923 and, 2872 cm$^{-1}$ can be attributed to stretching vibration of CH in $sp^3$ groups, the band at 1706 and 1676 cm$^{-1}$ can be attributed to stretching vibration of carbonyl groups.

Bands at 1108 and 1052 cm$^{-1}$ showed stretching vibration of C-O groups. The peak at 989 cm$^{-1}$ is attributed to C-H bending absorption, and the strong peak at 758 cm$^{-1}$ is attributed to benzene rings C-H vibration absorption.

A peak at 689 cm$^{-1}$ is attributed to the vibration absorption of alkenes. The spectrum of nanoemulsion without *C. aurantium* EO displayed in Figure 3B, the broad peak at about 3493 cm$^{-1}$ can be attributed to OH stretching vibration due to hydrogen bonding between water and tween 20. Spectra at 2924 cm$^{-1}$ corresponded to C-H stretching in tween 20. A strong band at 1733 cm$^{-1}$ attributed to C=O stretching, representing the carbonyl group in tween 20.

Characteristic band at around 1462 cm$^{-1}$ can be attributed to $CH_2$ bending tween 20. Characteristic and sharp peak at 1091 cm$^{-1}$ is assigned to C-O stretching. FTIR of *C. aurantium* EO nanoemulsion spectrum (Figure 3C) showed the broadband at 3518 cm$^{-1}$ attributed to OH stretching vibration due to the strong hydrogen bonding between water, tween 20, and phenolic and alcoholic compounds in EO. Any band at 2969, 2924, and 2856 cm$^{-1}$ is related to C-H stretching due to $sp^3$ hybrid in tween 20 and EO. Strong band at 1728 cm$^{-1}$ showed carbonyl stretching (C=O) tween 20 and EO. The absorption at around 1456 cm$^{-1}$ corresponded to $CH_2$ bending tween and EO. A sharp and strong peak at about 1093 cm$^{-1}$ can be attributed to C-O stretching.

Spectrum of the *A. annua* EO has been demonstrated in Figure 3D, a broad and characteristic band at about 3520 cm$^{-1}$, can be attributed to the hydroxyl functional groups in EO, and a band at 3084 cm$^{-1}$, allocated to the stretching vibration of =C-H groups from olefins in $sp^2$ hybrid. Peaks at 2963, 2928, and 2872 cm$^{-1}$, related to stretching vibrations of –CH in $sp^3$ hybrid, the spectra at around 1743 cm$^{-1}$ related to C=O, the absorption around 1620 and 1415 cm$^{-1}$ assigned to C = C, the bands at 1215 and 1167 cm$^{-1}$ are related to (C-O-C) bonds and the band at 876 cm$^{-1}$ can be allocated to angular deformations of $CH_2$ groups. Spectra of nanoemulsion without *A. annua* EO has been shown in Figure 3E.

A characteristic and broad peak between 3200 to 3600 cm$^{-1}$ corresponds to OH stretching vibration due to the hydrogen bonding between water and tween 80. Spectra at 2964 and 2925 cm$^{-1}$ are related to C-H stretching. Absorption at 1740 cm$^{-1}$ was attributed to carbonyl stretching (C=O) in tween 80 and at about 1456 cm$^{-1}$ can be allocated to $CH_2$ bending. A strong and characteristic band at 1080 cm$^{-1}$ corresponded to C-O stretching.

ATR-FTIR of nanoemulsion containing *A. annua* EO has been displayed in Figure 3F. A peak at about 3422 cm$^{-1}$ is attributed to OH stretching vibration due to hydrogen bonding between EO, tween 80, and water and at 2924 cm$^{-1}$ corresponds to C-H stretching of EO and tween 80. Absorption at 1733 cm$^{-1}$ attributed to C=O stretching representing the carbonyl group in EO and tween. A characteristic peak at about 1462 cm$^{-1}$ outlined $CH_2$ bending in EO and tween 80. A strong and sharp peak at 1091 cm$^{-1}$ was assigned to C-O stretching. The presence of other bands in EOs and blanks confirmed the successful loading of EOs in the prepared nanoemulsion.

The *C. aurantium* and *A. annua* nanoemulsions were evaluated for their antioxidant effects by DPPH assay. As shown in Figure 4, the most potent free radical scavenging activity was obtained from *A. annua* EO nanoemulsion, 40 % at 2000 µg/mL.

### 3.3. The Minimum Inhibitory Concentration (MIC) and Minimum Bactericidal Concentration (MBC)

According to Table 3, the *C. aurantium* EO nanoemulsion MIC against *S. aureus*, *E. coli*, *P. aeruginosa*, and *K. pneumonia* included 500 µg/mL, 1000 µg/mL, 1000 µg/mL, and 1000 µg/mL, respectively. The MBC values against bacterial strains also included >2000µg/mL. Moreover, the MIC values of *A. annua* nanoemulsion EO against *S. aureus*, *E. coli*, *P. aeruginosa*, and *K. pneumonia* included 1000 µg/mL, 2000 µg/mL, 2000 µg/mL, and 2000 µg/mL, respectively. The MBC values included >2000 µg/mL for all the tested bacterial strains.

### 3.4. Antibacterial Effects

The bacterial growth inhibitory effect of *C. aurantium* nanoemulsion EO was concentration-dependent. The highest bactericidal effect was observed against *S. aureus* at 2000 µg/mL, in which 56% of growth was inhibited (Figure 5).

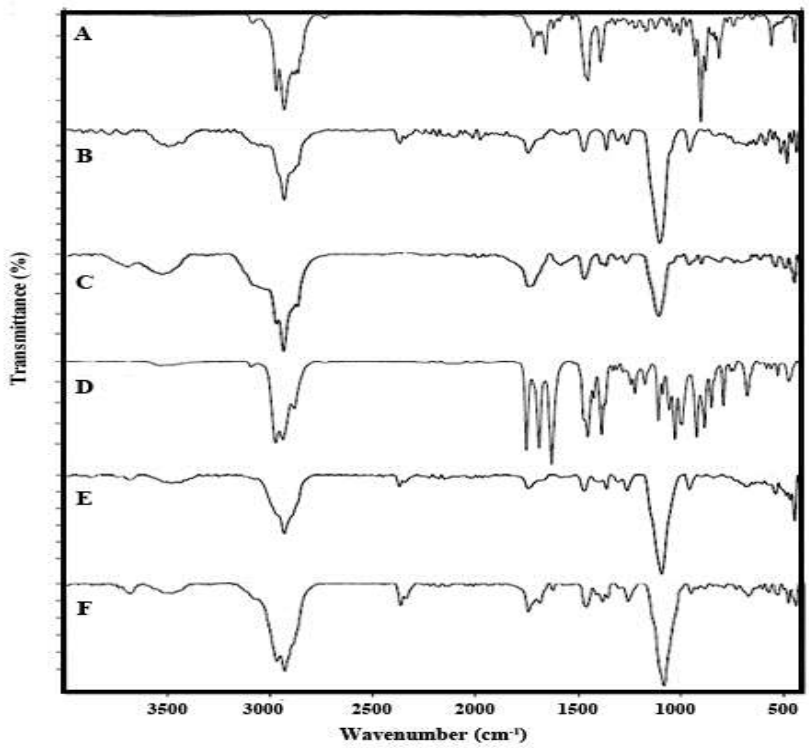


**Figure 3.** ATR-FTIR spectra of A: *C. aurantium* EO, B: nanoemulsion without *C. aurantium* EO, C: nanoemulsion containing *C. aurantium* EO, D: *A. annua* EO, E: nanoemulsion without *A. annua* EO, F: nanoemulsion containing *A. annua* EO.

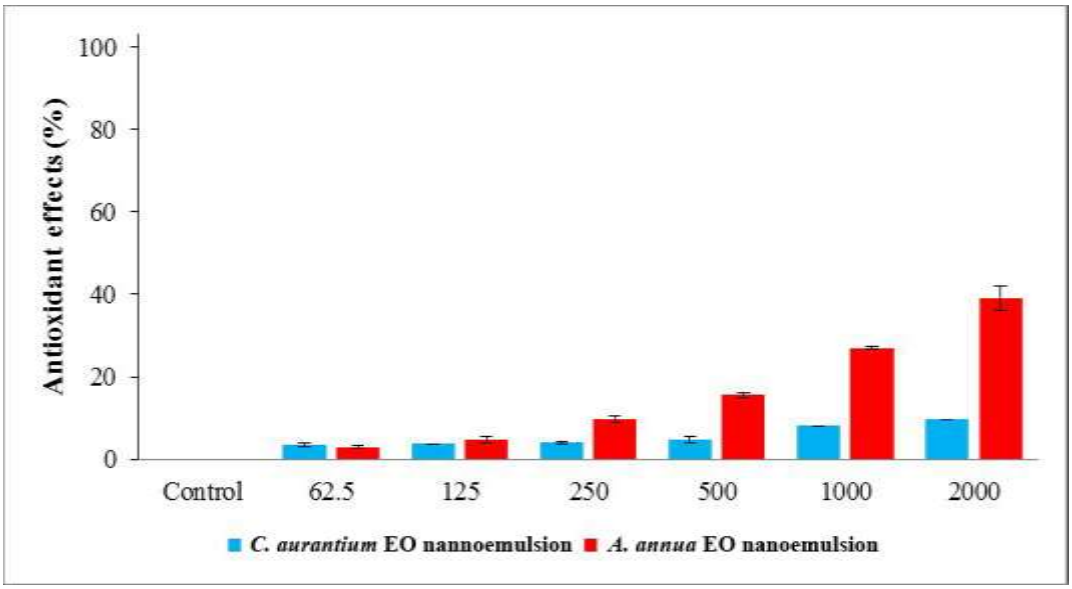


**Figure 4.** The antioxidant effects of samples.

**Table 3.** The MIC and MBC levels (µg/mL) samples.

| Samples | *S. aureus* (MIC, MBC) | *E. coli* (MIC, MBC) | *P. aeruginosa* (MIC, MBC) | *K. pneumonia* (MIC, MBC) |
|---|---|---|---|---|
| ***C. aurantium* EO nanoemulsion** | 500, >2000 | 1000, >2000 | 1000, >2000 | 1000, >2000 |
| ***A. annua* EO nanoemulsion** | 1000, >2000 | 2000, >2000 | 2000, >2000 | 2000, >2000 |

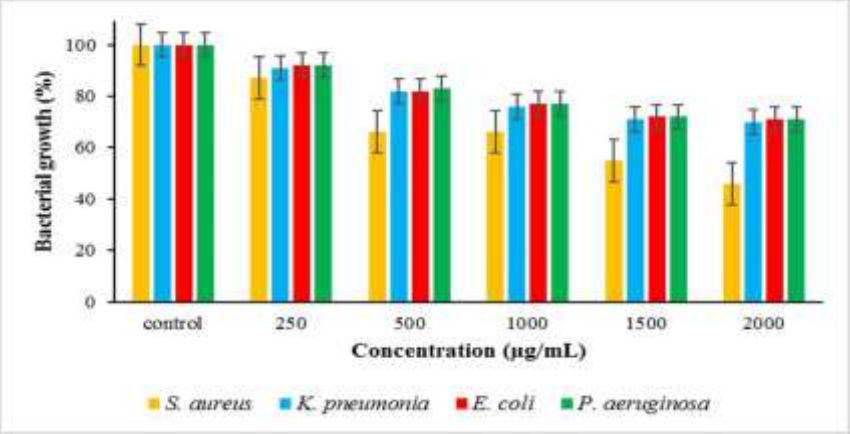


**Figure 5.** The bacterial growth in exposure to *C. aurantium* nanoemulsion EO.

The growth inhibitory effect of *A. annua* nanoemulsion EO was mostly against *S. aureus* at 2000 µg/mL, in which ~20 % of bacterial growth was inhibited (Figure 6).

### 3.5. Anti-biofilm effects

As shown in Figure 7, biofilms in the control group all bacteria were formed (OD > 0.083). However, after treatment with both nanoemulsions, no biofilm (OD < 0.083) was formed by all examined bacteria, i.e., *S. aureus*, *K. pneumonia*, *E. coli*, and *P. aeruginosa*.

## 4. Discussion

In our study, nanoemulsions of *C. aurantium* and *A. annua* EOs were prepared using spontaneous emulsification. Their antimicrobial and antibiofilm against selected bacterial pathogens were subsequently investigated. While previous studies have investigated antimicrobial and insecticidal properties of *C. aurantium* and *A. annua* extracts and EOs against different microorganisms, but our study has focused mostly on their nanoemulsion forms (20).

For example, Kačániová et al examined the biological activity and antibiofilm molecular profile of *C. aurantium* EO, concluding that *C. aurantium* EO exhibited potent antibacterial activity against *Stenotrophomonas maltophilia* and *Bacillus subtilis*, followed by *Penicillium crustosum* (15). In addition, Madhuri et al reported that EOs extracted from the peel of *C. aurantium*can be used against infectious agents such as *K. pneumonia* and *Bacillus cereus* (21).

*In vitro* studies by Marinas et al. also showed that *A. annua* EO has selective antipathogenic activity on Gram-positive and Gram-negative bacterial strains (22).

Its antibacterial and anti-biofilm activities have been also unveiled (23, 24). In addition, Mariadosset et al. synthesized the selenium nanoparticles using *A. annua* (AaSeNPs) of 109.2 nm in size and the characterized AaSeNPs indicated an antibacterial activity against multidrug-resistant pathogens such as *S. aureus*, *B. subtilis*, *Proteus mirabilis*, and *E. coli* (25). Das et al. also reported stronger antimicrobial activity of Pickering nanoemulsion of the *Artemisia* essential oil (24).

In our study, antimicrobial and antibiofilm effects of nanoemulsions of *C. aurantium* and *A. annua* EOs against selected bacterial pathogens were confirmed through MIC and MBC tests with the highest activity against *S. aureus*. Exposure of pathogens to the nanoemulsions resulted in a significant reduction in the biofilm formation by all examined bacteria, i.e., *S. aureus*, *K. pneumonia*, *E. coli*, and *P. aeruginosa*. This study is the first to investigate the chemical composition of *C. aurantium* and *A. annua* EO in detail, followed by the preparation of their nanoemulsion dosage forms.

The antimicrobial and antibiofilm activities of these nanomulsions were demonstraed. Both nanoemulsions inhibited the growth of *S. aureus* and notably, no biofilm formations by *S. aureus*, *K. pneumonia*, *E. coli*, and *P. aeruginosa* were observed after treatment with these nanoemulsions.

Moreover, *A. annua* nanoemulsion inferred potent antioxidant properties. Limitations of this study mostly included the low number of bacterial pathogens, the absence of *in silico* assessment of binding of bioactive compounds to bacterial targets and the lack of *in vivo* study.

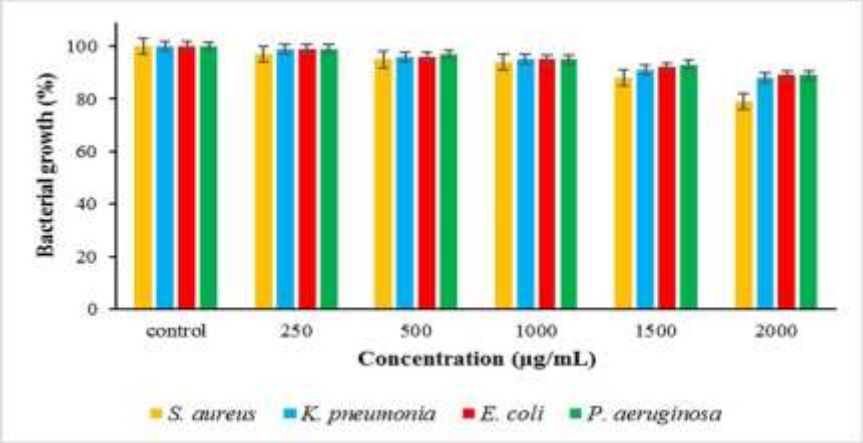


**Figure 6.** The bacterial growth in exposure to *A. annua* nanoemulsion EO.

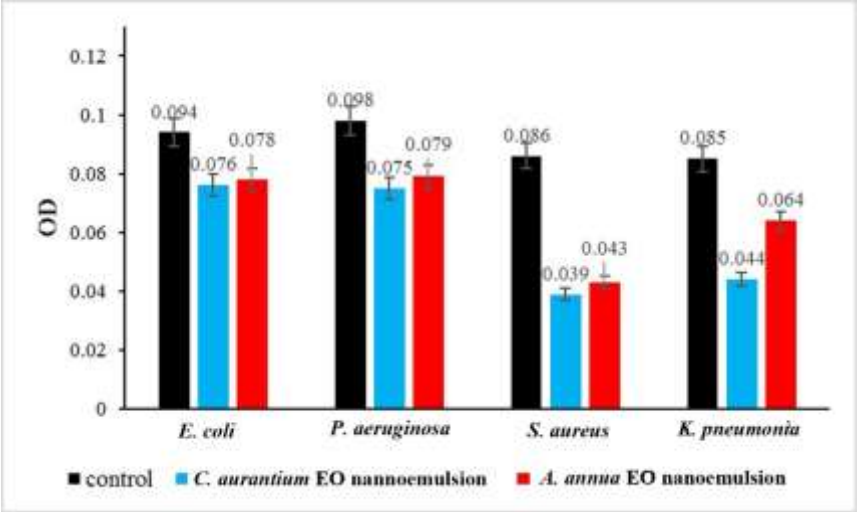


**Figure 7.** The anti-biofilm effects of (mean OD value) samples.

**Acknowledgment**

This study was supported by Fasa University of Medical Sciences.

**Authors' Contribution**

Study concept and design: MO, AG, ATR-FTIR.
Acquisition of data: AG, MS.
Analysis and interpretation of data: HA, EZ.
Drafting of the manuscript: MS, MO.
Critical revision of the manuscript for important intellectual content: MAH, BM.
Statistical analysis: DPPH, MO.
Administrative, technical, and material support: MS, AG.

**Ethics**

This study was supported by Fasa University of Medical Sciences under grant No. 401268 and was ethically approved (IR.FUMS.REC.1401.205).

**Conflict of Interest**

None.

**Funding**

Fasa University of Medical Sciences supported this study.

**Data Availability**

The data supporting the findings of this study are available from the corresponding author upon request.

## References

1. Mestrovic T, Aguilar GR, Swetschinski LR, Ikuta KS, Gray AP, Weaver ND, et al. The burden of bacterial antimicrobial resistance in the WHO European region in 2019: A cross-country systematic analysis. The Lancet Public Health. 2022;7(11):e897-e913
2. Laxminarayan R. The overlooked pandemic of antimicrobial resistance. The Lancet. 2022;399(10325):606-7
3. Noorpisheh Ghadimi S, Sharifi N, Osanloo M. The leishmanicidal activity of essential oils: A systematic review. Journal of Herbmed Pharmacology. 2020;9(4):300-8.https://doi.org/10.34172/jhp.2020.38
4. Qasemi H, Fereidouni Z, Karimi J, Abdollahi A, Zarenezhad E, Rasti F, et al. Promising antibacterial effect of impregnated nanofiber mats with a green nanogel against clinical and standard strains of Pseudomonas aeruginosa and Staphylococcus aureus. Journal of Drug Delivery Science and Technology. 2021.
5. Kanwar R, Rathee J, Salunke DB, Mehta SK. Green nanotechnology-driven drug delivery assemblies. ACS omega. 2019;4(5):8804-15
6. Swain SS, Paidesetty SK, Padhy RN, Hussain T. Nano-technology platforms to increase the antibacterial drug suitability of essential oils: A drug prospective assessment. OpenNano. 2022:100115
7. Rahchamani R, Zarooni S, Borhani MS. The Chemical Composition and Antibacterial Effect of Essential Oils of Rosemary and Basil in Milk. Iranian Journal of Veterinary Medicine. 2024
8. Farzaneh M, Fadaei V, Gandomi H. Antioxidant, Syneresis, and Sensory Characteristics of Probiotic Yogurt Incorporated With Agave tequilana Aqueous Extract. Iranian Journal of Veterinary Medicine. 2023;17(3):243-52
9. Ali Anvar SA, Nowruzi B, Afshari G. A Review of the Application of Nanoparticles Biosynthesized by Microalgae and Cyanobacteria in Medical and Veterinary Sciences. Iranian Journal of Veterinary Medicine. 2023;17(1)
10. Khaji L, Noori N, Jebelli Javan A, Khanjari A, Ghandomi Nasrabadi H. antimicrobial effect of Cuminum Cyminum essential oil on Iranian white soft cheese in air and modified atmosphere packaging during refrigerated storage. Iranian Journal of Veterinary Medicine. 2023
11. Maksoud S, Abdel-Massih RM, Rajha HN, Louka N, Chemat F, Barba FJ, et al. Citrus aurantium L. Active Constituents, Biological Effects and Extraction Methods. An Updated Review. Molecules. 2021;26(19).https://doi.org/10.3390/molecules26195832.
12. Gao L, Zhang H, Yuan CH, Zeng LH, Xiang Z, Song JF, et al. Citrus aurantium 'Changshan-huyou'-An ethnopharmacological and phytochemical review. Front Pharmacol. 2022;13:983470.
13. Liu S, Lou Y, Li Y, Zhang J, Li P, Yang B, et al. Review of phytochemical and nutritional characteristics and food applications of Citrus L. fruits. Front Nutr. 2022;9:968604.https://doi.org/10.3389/fnut.2022.968604.
14. Okla MK, Alamri SA, Salem MZ, Ali HM, Behiry SI, Nasser RA, et al. Yield, phytochemical constituents, and antibacterial activity of essential oils from the leaves/twigs, branches, branch wood, and branch bark of Sour Orange (Citrus aurantium L.). Processes. 2019;7(6):363
15. Kačániová M, Terentjeva M, Galovičová L, Ivanišová E, Štefániková J, Valková V, et al. Biological activity and antibiofilm molecular profile of Citrus aurantium essential oil and its application in a food model. Molecules. 2020;25(17):3956
16. Anibogwu R, Jesus K, Pradhan S, Pashikanti S, Mateen S, Sharma K. Extraction, Isolation and Characterization of Bioactive Compounds from Artemisia and Their Biological Significance: A Review. Molecules. 2021;26(22).https://doi.org/10.3390/molecules26226995.
17. Bilia AR, Santomauro F, Sacco C, Bergonzi MC, Donato R. Essential Oil of Artemisia annua L.: An Extraordinary Component with Numerous Antimicrobial Properties. Evid Based Complement Alternat Med. 2014;2014:159819.https://doi.org/10.1155/2014/159819.
18. Mirzaei-Najafgholi H, Tarighi S, Golmohammadi M, Taheri P. The Effect of Citrus Essential Oils and Their Constituents on Growth of Xanthomonas citri subsp. citri. Molecules. 2017;22(4):591
19. Osanloo M, Ghaznavi G, Abdollahi A. Sureveying the chemical composition and antibacterial activity of essential oils from selected medicinal plants against human pathogens. Iranian Journal of Microbiology. 2020;12(6):505-12
20. Durán Aguirre CE, Pratissoli D, Damascena AP, Romário de Carvalho J, de Araujo Junior LM. Lethal and sublethal effects of Citrus aurantium and Citrus sinensis essential oils and their major component limonene on Helicoverpa armigera (Hübner) (Lepidoptera: Noctuidae). Journal of Essential Oil Bearing Plants. 2024;27(3):838-48.https://doi.org/10.1080/0972060X.2023.2286259.
21. Madhuri S, Hegde AU, Srilakshmi N, Prashith Kekuda T. Antimicrobial activity of Citrus sinensis and Citrus aurantium peel extracts. Journal of Pharmaceutical and Scientific Innovation (JPSI). 2014;3(4):366-8
22. Marinas IC, Oprea E, Chifiriuc MC, Badea IA, Buleandra M, Lazar V. Chemical composition and antipathogenic activity of Artemisia annua essential oil from Romania. Chemistry & Biodiversity. 2015;12(10):1554-64
23. Al-Mothafar NA, Al-Shahwany AW. Phenolic compounds from Thymus vulgaris, Artemisia annua extracts and pure Thymol were tested against twenty Pseudomonas spp. strains for antibacterial and anti-biofilm activities. IOP Journal of Physics Under review.
24. Das S, Vörös-Horváth B, Bencsik T, Micalizzi G, Mondello L, Horváth G, et al. Antimicrobial activity of different Artemisia essential oil formulations. Molecules. 2020;25(10):2390
25. Mariadoss AVA, Saravanakumar K, Sathiyaseelan A, Naveen KV, Wang M-H. Enhancement of anti-bacterial potential of green synthesized selenium nanoparticles by starch encapsulation. Microbial Pathogenesis. 2022;167:105544